MATERIALS SCIENCE

Self-adaptive photochromism

Fanxi Sun[1], Ang Gao[1], Boyun Yan[1], Jing Zhang[1], Xiangru Wang[1], Hanjun Zhang[1], Dacheng Dai[1], Yonghao Zheng[1]*, Xu Deng[2], Chen Wei[1]*, Dongsheng Wang[1]*

Organisms with active camouflage ability exhibit changeable appearance with the switching of environments. However, manmade active camouflage systems heavily rely on integrating electronic devices, which encounters problems including a complex structure, poor usability, and high cost . In the current work, we report active camouflage as an intrinsic function of materials by proposing self-adaptive photochromism (SAP). The SAP materials were fabricated using donor-acceptor Stenhouse adducts (DASAs) as the negative photochromic phases and organic dyes as the fixed phases (nonphotochromic). Incident light with a specific wavelength induces *linear*-to-*cyclic* isomerization of DASAs, which generates an absorption gap at the wavelength and accordingly switches the color. The SAP materials are in the primary black state under dark and spontaneously switch to another color upon triggering by transmitted and reflected light in the background. SAP films and coatings were fabricated by incorporating polycaprolactone and are applicable to a wide variety of surfaces.

INTRODUCTION

Camouflage is a common and important trait of animals, including disruptive coloration (*1*) (Commerson's frogfish), self-decoration (decorator crabs) (*2*), mimesis (flower mantis) (*3*), distraction (peacock butterfly) (*4*), and active camouflage (chameleon and octopus) (*5*–*8*). Among them, active camouflage enables organisms to actively alter their appearance to blend into their surroundings, making the organisms difficult to recognize in different environments. This camouflage skill could be achieved by manmade systems through a sequential operation of recognize, process, stimulate, and change (Fig. 1A). The color of the environment is first recognized by a camera and then transformed into digital signals, which control stimuli (e.g., heat and electricity) to induce color switching of materials (*9*–*11*). These systems heavily rely on the integration of electronic devices, which brings problems such as a complex structure, poor usability, and high cost. To date, it remains challenging to achieve active camouflage based on the intrinsic functionality of color-switchable materials.

Our strategy is to make active camouflage an intrinsic function of materials. We propose self-adaptive photochromism (SAP), where the color of materials could be directly switched to and maintained the same as that of incident light. The design of SAP materials follows the theory of complementary colors (*12*). The material exhibits an even absorption band in the entire visible light region, corresponding to black, in the dark (Fig. 1B). After exposure to light irradiation with a specific wavelength, the absorbance at this wavelength decreases, generating a gap in the absorption spectrum (Fig. 1B). This further switches the color of the SAP materials to match that of the incident light. To realize SAP, photoswitches (photochromic molecules) are needed that meet the following requirements: (i) exhibits properties termed t-type (thermally reversible type) negative photochromism (*13*, *14*), characterized by the disappearance of the absorption band at corresponding wavelengths induced by visible light (resulting in color disappearance) and a thermal-dominated process for color recovery; and (ii) show a narrow and tunable absorption band in the visible light region.

[1]School of Optoelectronic Science and Engineering, University of Electronic Science and Technology of China, Chengdu 610054, China. [2]Institute of Fundamental and Frontier Science, University of Electronic Science and Technology of China, Chengdu 610054, China.
*Corresponding author. Email: zhengyonghao@uestc.edu.cn (Y.Z.); cwei@uestc.edu.cn (C.W.); wangds@uestc.edu.cn (D.W.)

RESULTS

Design of SAP materials

Donor-acceptor Stenhouse adducts (DASAs) are selected as the photoswitches, which exhibit *linear*-to-*cyclic* isomerization under triggering by visible light, while the reverse *cyclic*-to-*linear* isomerization is thermally induced (Fig. 1C) (*13*, *14*). The *cyclic* isomer could be either zwitterionic or nonzwitterionic based on the chemical structure of electron-donating moieties (*15*–*17*). The absorption spectra could be shifted by varying the electron-donating and electron-withdrawing moieties (*15*, *18*, *19*). For the construction of SAP materials, DASAs termed D1 (*20*) (Abs_{max} = 556 nm), D2 (Abs_{max} = 590 nm) (*15*), D3 (Abs_{max} = 614 nm) (*15*), and D4 (Abs_{max} = 645 nm) (*21*) were synthesized and used as the negative photochromic phases (Fig. 1D and fig. S1). Because of the push-pull nature of DASAs, blueshifting of the absorption spectra encounters obstacles and thus does not cover the entire visible light region (*14*). Thus, organic dyes (F1 to F4) (*13*, *22*) with absorption bands between ~300 and ~550 nm were used as the fixed phases (nonphotochromic phases) (Fig. 1D and fig. S1). Notably, the fixed phases do not show photochromism. The absorption spectra of the negative photochromic and fixed phases are distributed between 300 and 700 nm with average intervals of ~40 nm, making the color of SAP materials precisely tunable in the visible light region.

All the DASAs exhibit a sharply decreased absorption band in the visible light region with the *linear*-to-*cyclic* isomerization, which results in colored-to-colorless switching (fig. S2, C to F). The reverse *cyclic*-to-*linear* isomerization spontaneously occurs in the dark (*23*). Typically, D4, with $-CF_3$ substituted electron-withdrawing group, shows fast thermal relaxation, which induces an increase in the absorbance band during the scanning of spectra (fig. S2F) (*18*). DASAs are in an equilibrium state (photostationary state) between *linear* and *cyclic* under light irradiation, and the *linear* content closely interrelated with the light conditions (i.e., wavelength and intensity) determines the color of SAP materials. To effectively evaluate the equilibrium states and the resulting colors for each DASA, specific light sources are required. Light-emitting diodes (LEDs) with emission wavelengths of 520 nm (green), 590 nm (yellow), 620 nm (orange), and 660 nm (red) were selected to switch the color of the SAP materials. The dynamics of the photoisomerization of DASAs under LED triggering were investigated to determine the *linear* content at

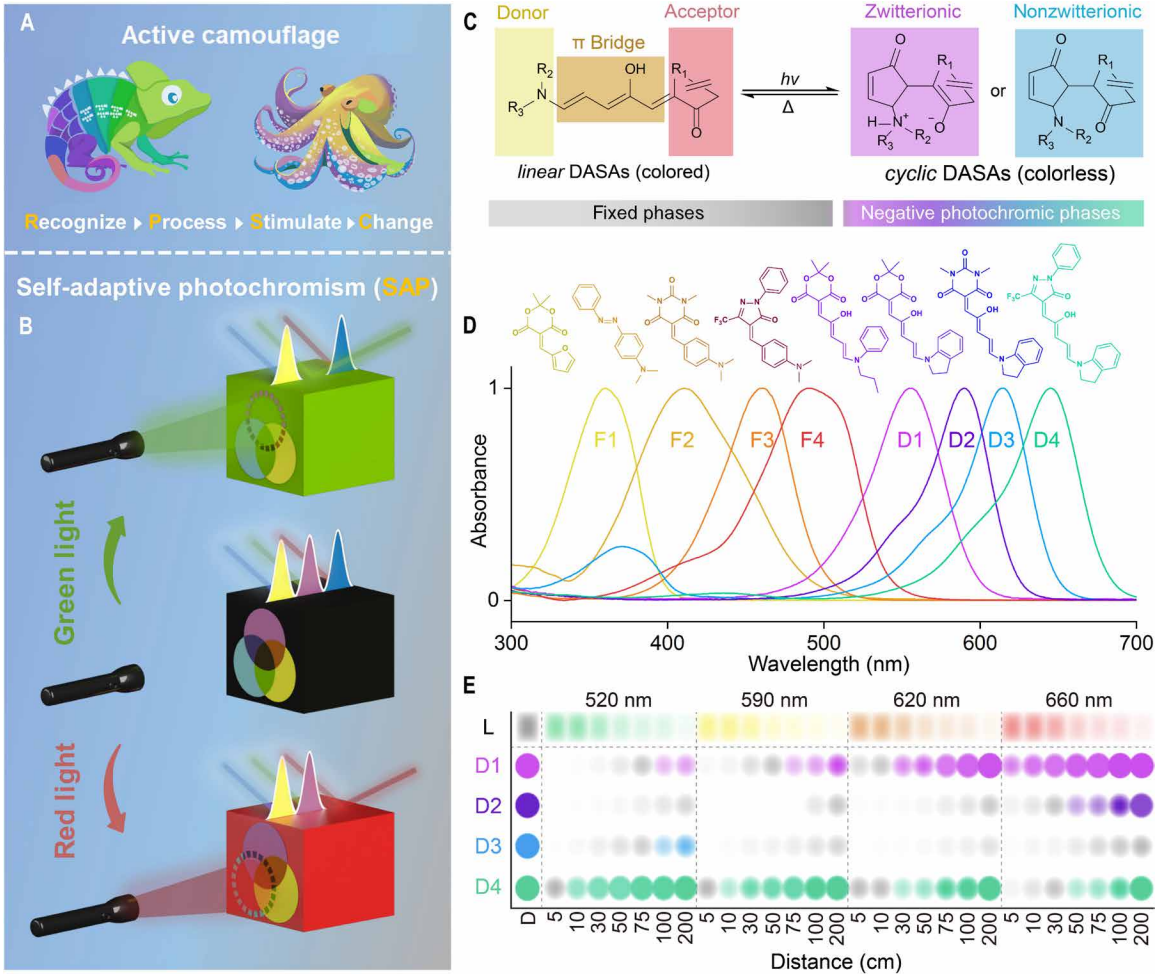

Fig. 1. Design of SAP materials. (**A**) Creatures with active camouflage (created with Photoshop 2023). (**B**) Schematic illustration of the mechanism of self-adaptive photochromism (SAP). (**C**) General chemical structure and isomerization between *linear* and *cyclic* donor-acceptor Stenhouse adducts (DASAs). (**D**) Normalized ultraviolet-visible (UV-vis) absorption spectra of the color-contributing units in fixed and negative photochromic phases [polycaprolactone (0.1 g/ml) in tetrahydrofuran/dichloromethane, 1:9 v/v]. (**E**) Relative color of DASAs under light irradiation with different wavelengths and distances.

equilibrium. The intensity of the irradiation was adjusted by controlling the distance between the LEDs and samples, ranging between 5 and 200 cm (fig. S3A). With increasing distance, the intensity of the light irradiation monotonically decreases (fig. S2A and table S1).

DASA solutions in a mixture of tetrahydrofuran (THF), dichloromethane (DCM), and polycaprolactone (PCL) were used. The *linear*-to-*cyclic* isomerization of all the DASAs follows first-order kinetics, and the *linear* content at equilibrium (L_e) could be obtained by fitting through the following equation (fig. S3B and table S32) (*15*, *24*)

$$L = L_e + L_1 \times e^{\left(-\frac{t}{t_0}\right)} \quad (1)$$

In the one-phase exponential decay function, L_e refers to the steady-state proportion of the *linear* content (%) of a DASA under constant light irradiation, while L represents the varying proportion of *linear* form during irradiation, and t_0 indicates the time required to reach the equilibrium. The fitted *linear* content at equilibrium for the DASAs under light irradiation with various wavelengths and intensities is shown in fig. S3B and table S32. To make the tendency visual, the data of the *linear* content were transformed into color information and are summarized in Fig. 1E, which quantifies the color contribution (considered 100% under dark conditions) of different DASAs under varying lighting conditions. With the decreasing distance between the LEDs and samples, the *linear* content exhibits a monotonic decrease for all the DASAs (fig. S3B). This results in the colorless appearance of DASAs (Fig. 1E). The matching between the absorbance spectra of DASAs and the emission spectra of LEDs is critically important for the promotion of photoisomerization. When the DASAs are irradiated by green light (distance, ≤75 cm), D1, D2, and D3 exhibit a *cyclic*-rich equilibrium state (*linear* content, <10%); in contrast, most of D4 is in the *linear* form (fig. S3B). Redshifting of the light increases the *linear* content of D1 and enriches the *cyclic* isomer of D4. However, D2 and D3 are mostly in the colorless *cyclic* form (*linear* content, <30%) under light irradiation between 520 and 660 nm (Fig. 1E and fig. S3B). These results might be attributed to the thermodynamically stable *cyclic* isomers of D2 and D3 (*15*, *24*–*26*). Therefore, D1 and D4 could be tuned over a wide range of lightness of color by controlling the wavelength and intensity of light, which contributes to the diversity of color for the SAP materials.

Color accuracy of SAP materials in the dark

For the construction of SAP materials, the constituents of the negative photochromic phases and fixed phases were optimized. The selection, ratio, and concentration of the organic dyes (F1 to F4) and DASAs (D1 to D4) were considered. We propose two general strategies (namely, A and R) to construct the SAP materials: (i) A, short for average, represents that all the color-contributing units show the same peak value of the absorbance spectra. For example, in the A4 strategy, the maximum absorption of each molecule is 1; (ii) R, short for ratio, represents that the ratio between the color-contributing units is controlled to keep the accumulated absorbance spectra as flat as possible. The compositions of the SAP materials include A2 (F4 + D4), A4 (F1 + F3 + D1 + D4), A6 and R6 (F1 + F2 + F3 + D1 + D2 + D4), A8, and R8.

The absorbance spectra of the SAP materials were obtained through the accumulation of each color-contributing unit using the following equation (Fig. 2A) (*27*)

$$A = a\varepsilon_{\mathrm{F1(360\ nm)}} + b\varepsilon_{\mathrm{F2(411\ nm)}} + c\varepsilon_{\mathrm{F3(461\ nm)}} + d\varepsilon_{\mathrm{F4(489\ nm)}} + e\varepsilon_{\mathrm{D1(556\ nm)}} + f\varepsilon_{\mathrm{D2(590\ nm)}} + g\varepsilon_{\mathrm{D3(614\ nm)}} + h\varepsilon_{\mathrm{D4(645\ nm)}} \quad (2)$$

The factors (a, b, c…) represent the contents (in micromolar) of color-contributing units, and ε_X (in per micromolar) represents the molar absorption coefficient obtained through the standard curve method (fig. S16 and table S2) (*28*). The composition of each SAP material is shown in table S33. The cumulative absorbance spectra were transformed into transmittance through $T = 10^{-A}$ (Fig. 2A). With an increasing number of color-contributing units, the SAP materials gradually exhibit even and quasi-full absorbance and transmittance bands in the visible light region.

To quantify the color information carried by the transmission spectra, a modified CIE 1931 color space (created by the International Commission on Illumination) (*29*) with a^* b^* coordinates was obtained through the transmittance spectra to quantitatively

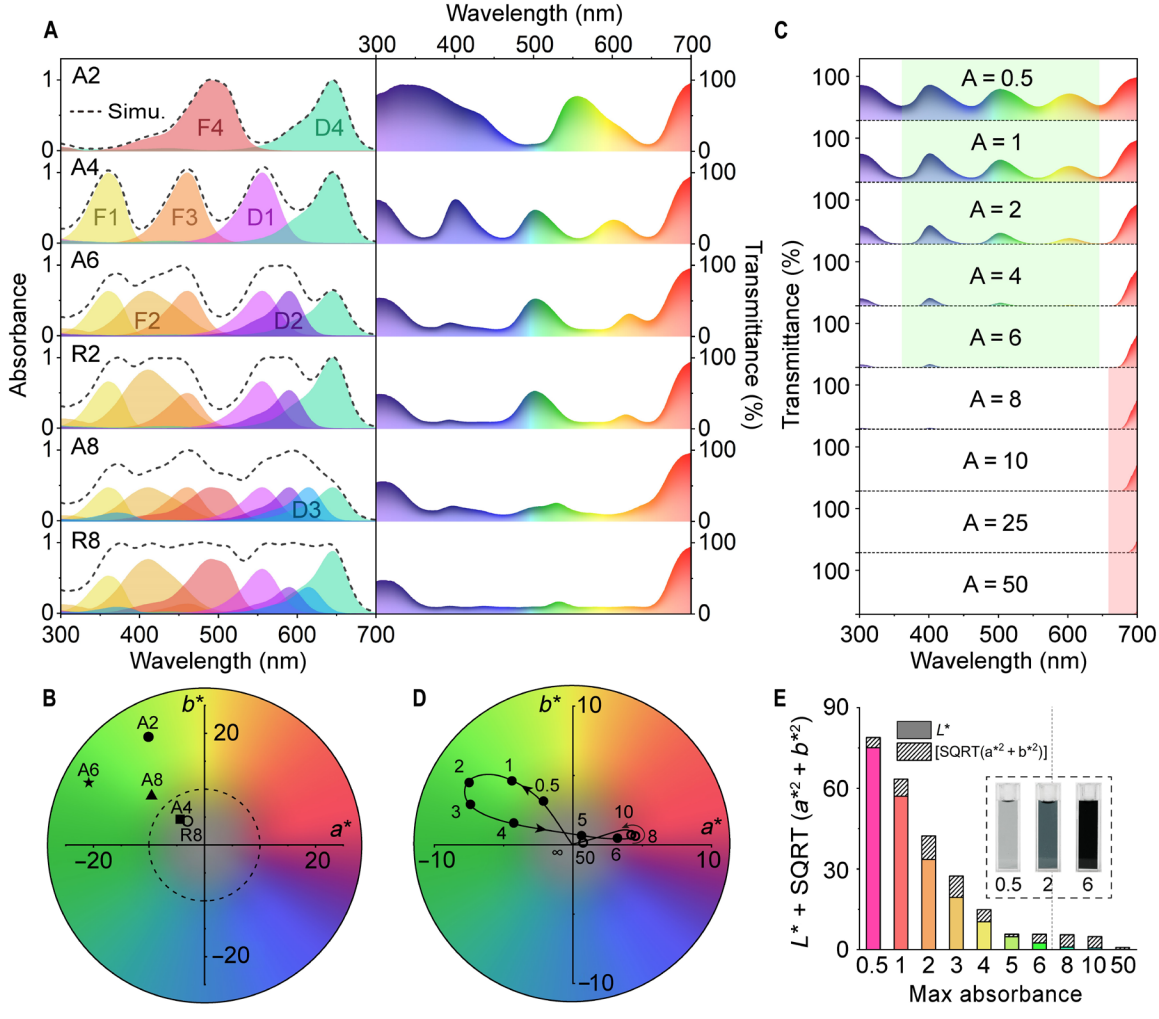

Fig. 2. Color accuracy of SAP materials in the dark. (**A**) Simulated UV-vis absorption (left) and transmission (right) spectra of SAP solutions with various combinations. (**B**) Modified CIE 1931 a^* b^* values of SAP solutions; the closer to the origin indicates that the SAP solutions show higher color accuracy in black. (**C**) Simulated UV-vis transmission spectra of A4 solutions with various initial absorbances. (**D**) Modified CIE 1931 a^* b^* values of A4 solutions with the initial absorbance increasing from 0.5 to 50. (**E**) Calculated brightness (L^*, colored solid) and deviation [SQRT(a^{*2} + b^{*2}), diagonal filled] values of the A4 solutions with initial absorbance between 0.5 and 50; the inset shows photographic images of A4 solutions with the initial absorbance of 0.5, 2, and 6. Lower L^*+ SQRT(a^{*2} + b^{*2}) indicates higher color accuracy in black.

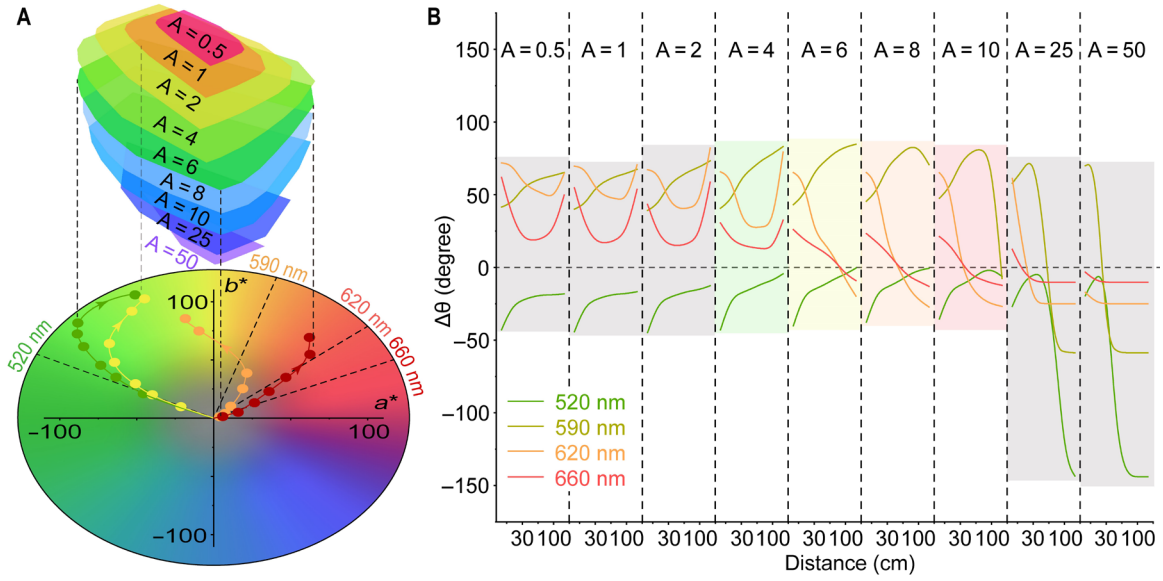

Fig. 3. Color accuracy of SAP materials under light irradiation. (**A**) Top half: Tunable range of color for A4 solutions with various initial absorbances. Down half: Modified CIE 1931 a^* b^* values of A4 solutions (A = 6) under 520-nm (green), 590-nm (yellow), 620-nm (orange), and 660-nm (red) light irradiation; the distance was kept at 5, 10, 30, 50, 75, 100, and 200 cm, and dash lines stand for the color of LED lights. (**B**) Modified CIE 1931 a^* b^* values of SAP solutions. (B) Accuracy of the color (Δθ) of A4 solutions under light irradiation with various conditions (wavelength and distance).

determine the color (Fig. 2B and table S34) (*30*). All the SAP materials show a greenish pristine color in the dark. R6 (−34.0, 8.3) is located outside the diagram due to the large absorption gap at approximately 460 to 520 nm (Fig. 2, A and B). Among them, A4 (−4.4, 4.6) and R8 (−3.1, 4.3) are close to the center of the diagram, indicating that the pristine color of these composites is sufficiently black. Quasi-full absorption of visible light is not essential to produce an accurate black color. A4 with a uniformly distributed absorption band exhibits high accuracy of black color as well as concise composition (Fig. 2A). Therefore, A4 was selected for the construction of SAP materials.

The concentration of the color-contributing units is closely interrelated with the lightness (L^*) of SAP materials. The initial absorbance of A4 was varied between 0.5 and 50 (fig. S4A). With increasing initial absorbance, the portion of transmitted light gradually decreases, while the transmittance spectrum switches from a uniformly distributed band (such as for A4) to an even band (such as for R8) (Fig. 2C). When the initial absorbance is kept between 0.5 and 4, the transmission light at 350 to 650 nm dominates the spectra, which results in a greenish pristine color for A4 (Fig. 2, B and C, and table S35). A further increase in the initial absorbance cuts off the transmission of green light, making A4 slightly reddish (Fig 2, C and D). The value of $L^* + \mathrm{SQRT}(a^{*2} + b^{*2})$ was calculated to quantitatively determine the color accuracy of the solution in black (Fig. 2E), where $\mathrm{SQRT}(a^{*2} + b^{*2})$ represents the color accuracy, L^* represents the brightness of the non-luminous measured object (*29*). A lower value of $L^* + \mathrm{SQRT}(a^{*2} + b^{*2})$ indicates that the pristine state of SAP materials is blacker. For A4 with a relatively low initial absorbance (0.5 to 4), L^* is the main factor affecting the color accuracy. An increase in the initial absorbance induces a monotonic and sharp decrease in L^*; in addition, the variation in $\mathrm{SQRT}(a^{*2} + b^{*2})$ is related to the initial absorbance (Fig. 2, D and E). With increasing initial absorbance, A4 gradually switches from light gray (A = 0.5) to deep green (A = 2) and black (A = 6), which corresponds well to the results in Fig. 2 (C and E). Consequently, the initial absorbance needs to be greater than 4 to ensure an accurately black pristine state for the SAP materials.

Color accuracy of SAP materials under light irradiation

The color accuracy of the SAP materials under light irradiation was simulated. A4 with an initial absorbance between 0.5 and 50 was considered. The simulation was based on the *linear* content of DASAs at equilibrium under light irradiation (Fig. 1E and fig. S3B). The photoisomerization of DASAs has been reported to show a concentration dependence, where the *linear* content at equilibrium increases with increasing concentration (*31*–*33*). Under the same light conditions, we found that the *linear* content did not obviously change for the DASA solutions with initial absorbances ranging from 1 to 25 (fig. S18). The absorption and transmission spectra of A4 under light irradiation with different wavelengths and intensities were calculated by accumulating the spectra of color-contributing units in the photostationary state (figs. S19 to S27). In the modified CIE 1931 color space, the color of incident light was expressed as a straight line through the center and in a specific direction (fig. S4, D and F) (*29*). Light irradiation shifts the dot representing the color of SAP materials toward the corresponding line. However, for all wavelengths of light, with decreasing distance, the color of A4 gradually deviates and tends to switch to yellow. These results might be attributed to the photoisomerization of both D1 and D4 under strong LED light (Fig. 1C and fig. S3B). A4 exhibits a tunable range of color, which first increases with increasing initial absorbance of the solution. After reaching the maximum at A = 6, the tunable range sharply decreases (Fig. 3A and fig. S4C).

To quantitatively determine the color accuracy, the absolute difference in the angle between the dot and line (Δθ) in the chromaticity diagram was calculated, representing the color discrepancy

between the sample and the standard color (color of incident light), as shown in Fig. 3B and tables S47 to S55. When irradiated with green light, the color of A4 gradually approaches that of the incident light with increasing distance (Fig. 3B). For the A4 solutions with an initial absorbance between 4 and 10, Δθ reaches 0 at distances greater than 100 cm, indicating that the color deviation could be eliminated. Meanwhile, A4 with an initial absorbance of 6 to 10 exhibits accurate orange and red colors under 620- and 660-nm light irradiation, respectively. Therefore, for the construction of SAP materials, accounting for color accuracy, A4 with an initial absorbance of 6 was selected.

SAP and active camouflage in solutions

The achievement of active camouflage through SAP materials is based on the transmitted and reflected light of the background, which shows a specific wavelength according to the color of the environment (Fig. 4A) (*34*). For example, when the SAP materials are placed in a green environment, the green transmitted and reflected light switches the SAP materials to green, which could thus be hidden in the background.

Before light irradiation, the SAP solutions show a black pristine state, which switches to red, green, and yellow under 660-, 520-, and 590-nm light irradiation (5 mW/cm^2) (Fig. 4B). Green light and red light generate gaps in the absorption spectra of the SAP solutions at 500 to 600 nm and 600 to 700 nm due to the *linear*-to-*cyclic* isomerization of D1 and D4, respectively. In contrast, 590-nm yellow light switches both D1 and D4 to the colorless *cyclic* state, and the resulting SAP solutions show the overlaid color of F1 and F3. The color switching of SAP materials between black, red, green, and yellow is reversible (Fig. 4C). No obvious loss of absorbance (645 nm for red, 556 nm for green, and 602 nm for yellow) was noticed (*15*), indicating that the SAP materials are stable under light irradiation.

The active camouflage of SAP materials was evaluated by setting them in environments with different background colors. Cubic boxes of black, red, green, and yellow were fabricated from acrylic boards. The transmission spectra of the boxes were recorded to determine the incident light information (fig. S5A). To investigate the materials' camouflage capabilities during background transition, two cuvettes filled with the SAP solution (left) and nonswitchable black ink as the control (right) were placed into the boxes. A white light LED (10,000 lux) was used as the light source for triggering photochromism and illumination. Both solutions were in the pristine state in the black box after 30 s (Fig. 4D and movie S1). Placing the cuvettes in the red box switched the SAP solution to red in 80 s, which became difficult to identify by the naked eye. The SAP solution changed to green and yellow in 110 and 50 s in the green and yellow boxes. After being set in the black box, the SAP solution switched back to the pristine state. In contrast, the black ink remained black throughout the whole process. Moreover, the acrylic boards could be used as filters set between the light and SAP materials, which accordingly switched the solutions to green, yellow, orange, and red (fig. S5B and movie S2). We used self-written color analysis software to quantitatively evaluate the performance of active camouflage of the SAP materials (the source code is available in the "Processing of the video" section in Supplementary Materials) (*35*, *36*). The average RGB values in the fixed areas A (SAP solution), B (background), and C (black ink) were collected, and the absolute differences of A-B and C-B (ΔA-B and ΔC-B) were calculated, as shown in Fig. 4D. The SAP solution exhibited a monotonically decreasing ΔA-B value with time in the red, green, and yellow boxes, indicating that the color gradually switched to the same color as the background. Therefore, the SAP materials could be hidden in the environment and exhibit active camouflage. In contrast, the ΔC-B value of the black ink did not change in any environment.

For real applications, the SAP materials were placed in red (*Cyclamen persicum*), green (*Epipremnum aureum*), and yellow (*Ginkgo*) bushes, and a white light LED was set to the left of the plants. The transmitted and reflected light in the bushes induced photochromism of the SAP materials, as shown in Fig. 4A and fig. S5D. The reflectance spectra of the leaves were recorded, as shown in fig. S5C, which well matched the absorbance spectra of the SAP materials. Taking *C. persicum* as an example, the leaves mainly reflect light above 600 nm, resulting in red incident light for the SAP materials. The SAP solutions gradually switched from black to red, green, and yellow in the bushes of *C. persicum*, *E. aureum*, and *Ginkgo*, respectively (Fig. 4E and movies S3 and S4). An outdoor experiment was conducted under sunlight (60,000 lux, 37°C, and bottles were stored in the dark and immersed in liquid nitrogen for 5 s before the experiments), in which umbrellas of green, yellow, orange, and red were used (fig. S6). The SAP solutions accordingly switched and could be hidden under the umbrella (fig. S6 and movies S5 and S6).

The above studies focus on the response of SAP materials in a monochromatic environment. We expect that the SAP materials could mimic surrounding patterns with different colors, which is attractive to real-world applications. The addition of PCL increases the viscosity of SAP solutions, which slows the diffusion of color-contributing units. The SAP solution was filled into a slender transparent tube (25-mm outer diameter, 0.8-mm wall thickness, 160-mm length), which was covered with sequentially arranged red, green, and yellow sticky notes (Fig. 4F). A white light LED was set on the top. With irradiation, the SAP solution gradually switched from black to polychromic, making the sticky notes difficult to recognize (Fig. 4F and movie S7). The SAP solution exhibited a periodic yellow-red-green arrangement, which well matched the color of the above sticky notes.

SAP in films and coatings

Photochromism in the solid state furthers the applications of SAP materials in the real world (*37*, *38*). PCL with a low glass transition temperature (−60°C) and rich ester functional groups is an important matrix to efficiently promote the isomerization between *linear* and *cyclic* DASAs. On the one hand, the rubbery state of PCL at room temperature provides sufficient free space for molecular isomerization; on the other hand, the rich ester groups thermodynamically promote the *linear*-to-*cyclic* isomerization of DASAs by facilitating the process of intermolecular proton transfer (*39*).

The SAP solution was spin-coated onto the surface of a glass substrate, and after gentle peeling off, an SAP film was fabricated. The SAP film was in the black pristine state and switched to red, green, and yellow after 660-, 520-, and 590-nm light irradiation (60 mW/cm^2), respectively (Fig. 5A and movie S8). Compared to the solution, the SAP film needs a higher intensity of light and a longer irradiation time for photochromism, which is attributed to the hindered photoisomerization of DASAs in the solid state (*37*, *38*). The reflectance spectra of the SAP film after light irradiation are recorded in Fig. 5A. Because of the fast thermally induced *cyclic*-to-*linear* isomerization of D4, the reflectance spectra of the SAP film after 660- and 590-nm light irradiation were difficult to capture (*18*). More than 50% of *cyclic* D4 relaxed to the *linear* form during the

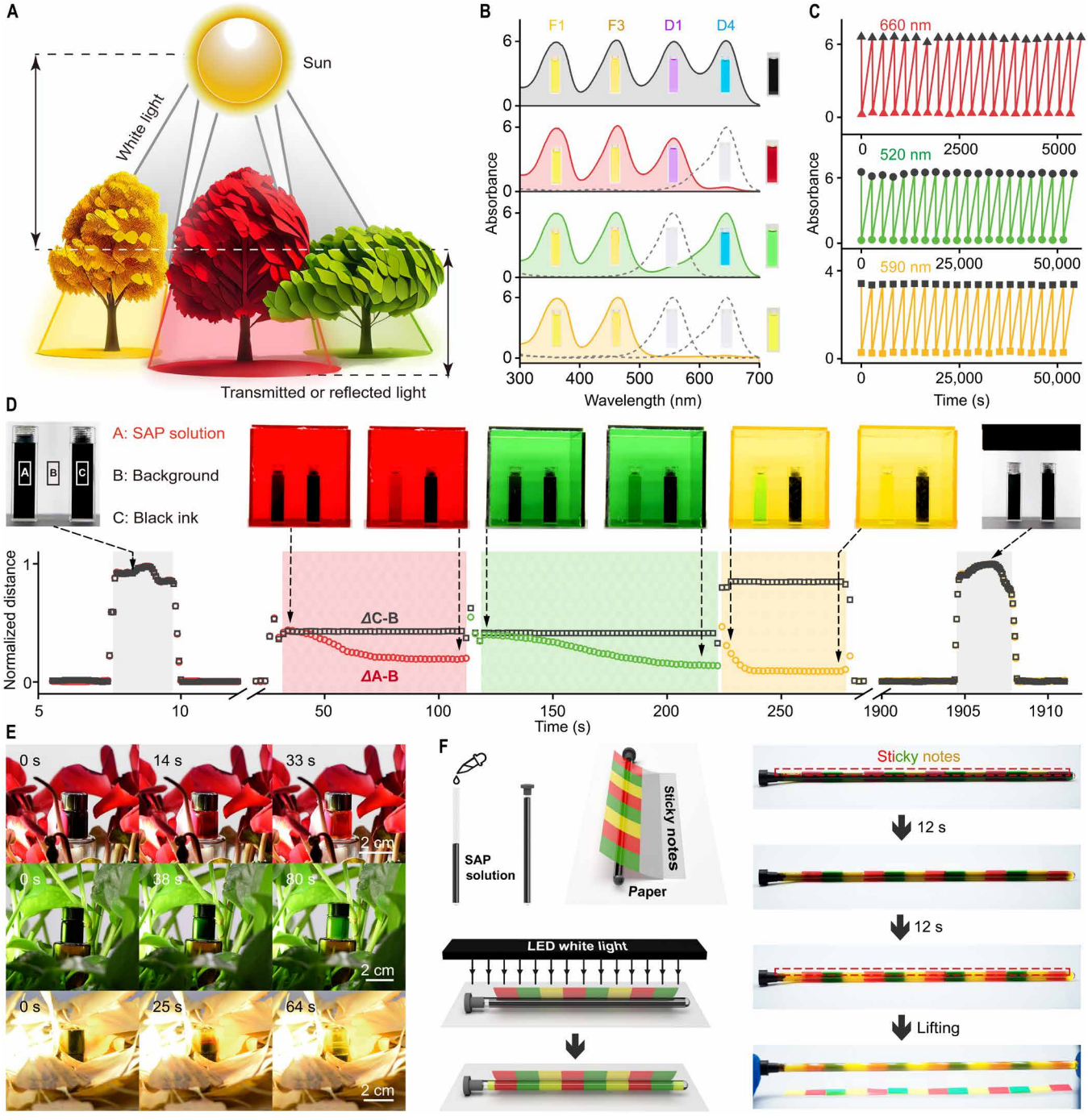

Fig. 4. SAP and active camouflage in solutions. (**A**) Schematic illustration of the philosophy for the active camouflage: The color of the environment depends on the transmitted and reflected light. (**B**) Normalized UV-vis absorption spectra of the SAP solutions in the dark and under 660-, 520-, and 590-nm light irradiation, inset shows the photographic images of each color-contributing unit and the resulted in SAP solutions (the spectra of 590- and 660-nm irradiation were obtained under the liquid nitrogen treatment). (**C**) Fatigue resistance of SAP solutions switching of black-red (red line, absorbance at 644 nm monitored), black-green (green line, absorbance at 556 nm monitored), and black-yellow (yellow line, absorbance at 602 nm monitored) for 20 cycles. (**D**) Color switching of SAP solutions in black, red, green, and yellow acrylic boxes; the left cuvette was loaded with SAP solutions, and the right cuvette with black ink as the control. Black dots represent the in situ distance between the average RGB values of regions C and B, and colored dots represent the distance between regions A and B. (**E**) Movie screenshots of the active camouflage of SAP solutions in red, green, and yellow bushes. (**F**) Schematic illustration and movie screenshots of realizing active camouflage by SAP solutions in a slender transparent tube (25-mm outer diameter, 0.8-mm wall thickness, 160-mm length) covered by sequentially arranged sticky notes.

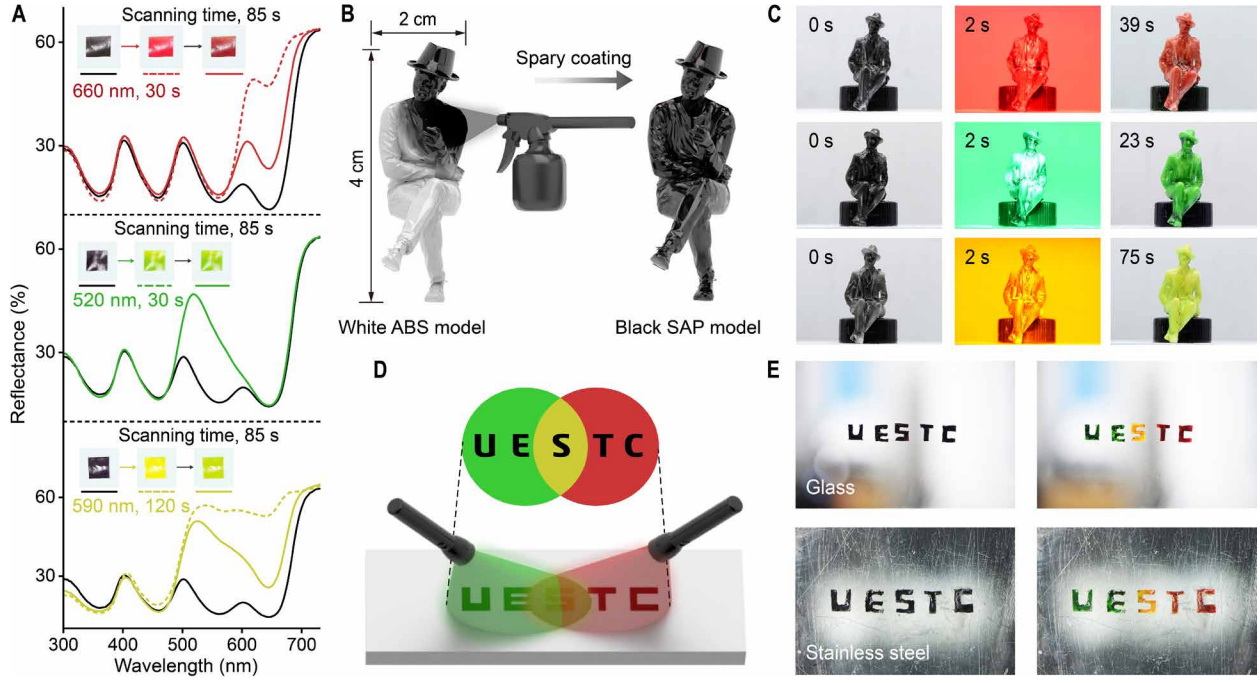

Fig. 5. SAP in films and coatings. (**A**) UV-vis diffuse reflectance spectra of SAP films before (black, solid) and after (colored) 660-nm (95 mW/cm^2, 30 s), 520-nm (140 mW/cm^2, 30 s), and 590-nm (25 mW/cm^2, 120 s) light irradiation; the spectra were recorded under room temperature (solid) and liquid nitrogen (dashed), and the insets show photographic images of the SAP films before irradiation, immediately after irradiation, and after 85-s scanning. (**B**) Schematic illustration of spray coating an SAP solution on the surface of a white acrylonitrile butadiene styrene (ABS) model. (**C**) Movie screenshots of the SAP process of three black ABS models in response to 660-nm (top), 520-nm (middle), and 590-nm (bottom) light. (**D**) Schematic illustration of irradiating the "UESTC" by green and red light. (**E**) Photographic images of SAP coatings on smooth surfaces (glass and stainless steel) before (left) and after (right) light irradiation.

scanning process (85 s), resulting in color deviation (solid line in Fig. 5A). Liquid nitrogen was used immediately after light irradiation to obtain the reflectance spectra of the SAP film (dashed line in Fig. 5A).

Coating is an attractive and important application for SAP materials. The SAP solution was spray coated onto the surface of a figurine model made of acrylonitrile butadiene styrene (ABS) plastic (Fig. 5B). A rapid annealing process generated a homogenously black and smooth surface of the figurine (figs. S29 and S30). Light irradiation at 660, 520, and 590 nm (60 mW/cm^2) was used to trigger photochromism of the SAP coating. The figurine switched to red, green, and yellow after light irradiation for 20 to 80 s (Fig. 5C and movie S9). Notably, the irradiation time for photochromism of the SAP coating is similar to that for the SAP film, where the 590-nm yellow light takes the longest time (Fig. 5, A and C) because the yellow light is located between the absorbance spectra of D1 and D4. The word "UESTC" (abbreviation for the University of Electronic Science and Technology of China) was recorded by spray coating the SAP solution through a mask (Fig. 5D and fig. S7A). Green and red LEDs were set separately on two sides of the substrate. The "UE" and "TC" were irradiated by green and red light, respectively. The "S" was simultaneously treated by green and red light, which resulted in yellow incident light. The SAP coating adapts well to a variety of surfaces, including glass, stainless steel, painted walls, A4 paper, wood, and clothes (Fig. 5E and fig. S7B). The black "UESTC" switched to polychromic after light irradiation, with green "UE," yellow "S," and red "TC." These results indicate that the SAP materials work well in the solid state.

DISCUSSION

In summary, we reported SAP of materials, where the color could be controllably switched to and maintained the same as that of incident light. DASAs (D1 to D4) and nonphotochromic organic dyes (F1 to F4) were used as the negative photochromic and fixed phases for the construction of SAP materials. On the basis of optimizing the selection, ratio, and concentration of the color-contributing units, A4 constituted by F1, F3, D1, and D4 was chosen for the construction of SAP materials, where the initial absorbance was kept at 6. In the solution state, the SAP materials switched to green, yellow, and red under 520-, 590-, and 660-nm light irradiation. Active camouflage was successfully achieved. In the environments with the background color of green (green acrylic box and umbrella, *E. aureum*), yellow (yellow acrylic box and umbrella, *Ginkgo*), orange (orange acrylic box and umbrella), and red (red acrylic box and umbrella, *C. persicum*), the SAP materials switched accordingly. Active camouflage works well in polychromic backgrounds with complex patterns. By applying PCL as the matrix, films and coatings were fabricated to demonstrate SAP in the solid state.

SAP materials show great potential to be applied in camouflage systems, smart coatings, and display devices. However, there are still some challenges that must be addressed. Because of the limitation of the chemical structure of DASAs, the absorbance spectra of SAP materials could be controlled above 520 nm (*14*). Therefore, purple and blue colors are missing from the current SAP materials. Future work could focus on developing negative photochromic molecules with an absorbance band in the blue light region. Overall, this work reported SAP as a distinct intrinsic property of materials, guiding

the development of source-free camouflage and anticounterfeiting technology.

MATERIALS AND METHODS

Materials

All the chemicals and reagents were used without further purification. 2-Furaldehyde ($C_5H_4O_2$, CAS no. 98-01-1), n-propylaniline ($C_9H_{13}N$, CAS no. 622-80-0), indoline (C_8H_9N, CAS no. 496-15-1), and sodium chloride (NaCl, CAS no. 7647-14-5) were purchased from Aladdin Chemicals (China). *n*-Hexane (C_6H_{14}, CAS no. 110-54-3), ethyl acetate ($C_4H_8O_2$, CAS no. 141-78-6), ethanol (C_2H_6O, CAS no. 64-17-5), methanol (CH_4OH, CAS no. 67-56-1), THF (C_4H_8O, CAS no. 109-99-9), and DCM (CH_2Cl_2, CAS no. 75-09-2) were purchased from General Reagent (China). 2,2-Dimethyl-1,3-dioxane-4,6-dione ($C_6H_8O_4$, CAS no. 2033-24-1) and 4-(dimethylamino)benzaldehyde ($C_9H_{11}NO$, CAS no. 100-10-7) were purchased from Adamas-Beta (China). Methyl yellow ($C_{14}H_{15}N_3$, CAS no. 60-11-7), petroleum ether (CAS no. 8032-32-4), and silicon dioxide (SiO_2, CAS no. 14808-60-7) were purchased from Chron Chemicals (China). 1,3-Dimethylbarbituric acid ($C_6H_8N_2O_3$, CAS no. 769-42-6) and PCL ($M_w = 80{,}000$) [$(C_6H_{10}O_2)_n$, CAS no. 24980-41-4] were purchased from HEOWNS Biochem Technologies LLC (China). 1-Phenyl-3-(trifluoromethyl)-1H-pyrazol-5(4H)-one ($C_{10}H_7F_3N_2O$, 321-07-3) was purchased from Bidepharm (China). Sodium sulfate (Na_2SO_4, CAS no. 15124-09-1) and sodium bisulfite ($NaHSO_3$, CAS no. 7631-90-5) were purchased from MERYER (China). Colored acrylic plates were purchased from Yixiang Plastic Co., Ltd (China). Colored sticky notes were purchased from Deli Group (China). ABS figurine models were purchased from the Yidemi toy store (China). The spraying coating set was purchased from Wudao Models (China). Milli-Q water (resistivity: 18.2 megohms·cm) was used throughout the project.

Characterization

Ultraviolet-visible (UV-vis) spectra (absorption, diffuse reflectance, and transmittance) were recorded on a Shimadzu UV-2600 spectrophotometer. The elemental mapping was performed on a field-emission scanning electron microscope (Carl Zeiss GeminiSEM 300) equipped with an energy-dispersive x-ray spectrometer. Single crystal x-ray diffraction was measured by a Gemini x-ray single crystal diffractometer. The LEDs of white light and visible light with the wavelengths of 520 (green), 590 (yellow), 620 (orange), and 660 nm (red) (Zhongjiao Jinyuan Systems) were used to induce the photoisomerization of DASAs and trigger the SAP. The output intensity of the LEDs was controlled by a controller (Zhongjiao Jinyuan Systems). The relationship between light intensity and distance of the LEDs was recorded on a PcPlug V3 (LaserPoint) and an AS823 Lux meter (Smart Sensor). The heat gun with the adjustable temperature ranging from room temperature to 650°C (AT-A822D, ATTEN) was used.

Synthesis

Below is a brief description of the synthesis methods for seven molecules; the detailed synthesis methods (fig. S1) and all crystal structures (figs. S9 to S15) were presented in the first section of the Supplementary Materials.

Synthesis of F1

F1 is synthesized by condensing 2,2-dimethyl-1,3-dioxane-4,6-dione with 2-furaldehyde in water. The mixture is heated to 40°C for 2 hours, resulting in a yellow solid. This solid is then purified through extraction with DCM and washing with aqueous solutions of sodium bisulfite and sodium chloride. The product is dried with sodium sulfate and further purified by column chromatography (*13*). For detailed procedures, see the "Synthesis" section in Supplementary Materials.

Synthesis of F3

F3 is obtained by condensing 1,3-dimethylbarbituric acid with 4-(dimethylamino)benzaldehyde in ethanol. The reaction mixture is heated to 90°C for 4 hours, yielding red precipitates upon cooling (*22*). For detailed procedures, see the "Synthesis" section in Supplementary Materials.

Synthesis of F4

F4 synthesis follows a similar procedure to F3, but instead of 1,3-dimethylbarbituric acid, 1-phenyl-3-(trifluoromethyl)-1H-pyrazol-5(4H)-one is used. The mixture is heated to 90°C for 4 hours, and the brown precipitates are collected after cooling (*22*). For detailed procedures, see the "Synthesis" section in Supplementary Materials.

Synthesis of D1

D1 is synthesized by reacting F1 with n-propylaniline in DCM. The reaction is stirred at 40°C and monitored by thin-layer chromatography. After rotary evaporation, the product is purified by column chromatography to yield a deep purple solid (*20*). For detailed procedures, see the "Synthesis" section in Supplementary Materials.

Synthesis of D2

D2 is synthesized by reacting F1 with indoline in DCM at 40°C for 2 hours. The reaction mixture is then treated with cold hexane to precipitate the purple solid, which is collected and further purified by column chromatography (*15*). For detailed procedures, see the "Synthesis" section in Supplementary Materials.

Synthesis of D3

D3 synthesis begins with the condensation of 1,3-dimethylbarbituric acid with 2-furaldehyde to form an intermediate. This intermediate is then reacted with indoline in DCM at 40°C. After rotary evaporation and treatment with cold hexane, the dark blue solid is collected and purified by column chromatography (*15*). For detailed procedures, see the "Synthesis" section in Supplementary Materials.

Synthesis of D4

D4 is synthesized by condensing 1-phenyl-3-(trifluoromethyl)-1 H-pyrazol-5(4H)-one with 2-furaldehyde in DCM at 40°C. The intermediate is then reacted with indoline in methanol at 20°C, resulting in the precipitation of green crystals. These crystals are filtered, washed with cold methanol, and dried to obtain D4 (*21*). For detailed procedures, see the "Synthesis" section in Supplementary Materials.

Supplementary Materials

The PDF file includes:

Supplementary Materials and Methods
Figs. S1 to S30
Tables S1 to S55
Legends for movies S1 to S9
Legends for data S1 and S2

Other Supplementary Material for this manuscript includes the following:

Movies S1 to S9
Data files S1 and S2

REFERENCES AND NOTES

1. T. W. Pietsch, D. B. Grobecker, Frogfishes. *Sci. Am.* **262**, 96–103 (1990).
2. K. Hultgren, J. Stachowicz, Camouflage in decorator crabs: Integrating ecological, behavioural and evolutionary approaches, in *Animal Camouflage* (Cambridge Univ. Press, 2011), pp. 214–229.

3. T. Mizuno, S. Yamaguchi, I. Yamamoto, R. Yamaoka, T. Akino, "Double-Trick" visual and chemical mimicry by the juvenile orchid mantis *Hymenopus coronatus* used in predation of the oriental honeybee *Apis cerana*. *Zool. Sci.* **31**, 795–801 (2014).
4. A. Vallin, S. Jakobsson, J. Lind, C. Wiklund, Prey survival by predator intimidation: An experimental study of peacock butterfly defence against blue tits. *Proc. R. Soc. B* **272**, 1203–1207 (2005).
5. M. Stevens, G. D. Ruxton, The key role of behaviour in animal camouflage. *Biol. Rev.* **94**, 116–134 (2019).
6. I. C. Cuthill, W. L. Allen, K. Arbuckle, B. Caspers, G. Chaplin, M. E. Hauber, G. E. Hill, N. G. Jablonski, C. D. Jiggins, A. Kelber, J. Mappes, J. Marshall, R. Merrill, D. Osorio, R. Prum, N. W. Roberts, A. Roulin, H. M. Rowland, T. N. Sherratt, J. Skelhorn, M. P. Speed, M. Stevens, M. C. Stoddard, D. Stuart-Fox, L. Talas, E. Tibbetts, T. Caro, The biology of color. *Science* **357**, eaan0221 (2017).
7. L. M. Mäthger, E. J. Denton, N. J. Marshall, R. T. Hanlon, Mechanisms and behavioural functions of structural coloration in cephalopods. *J. R. Soc. Interface* **6**, S149–S163 (2009).
8. J. Teyssier, S. V. Saenko, D. Van Der Marel, M. C. Milinkovitch, Photonic crystals cause active colour change in chameleons. *Nat. Commun.* **6**, 6368 (2015).
9. H.-H. Chou, A. Nguyen, A. Chortos, J. W. F. To, C. Lu, J. Mei, T. Kurosawa, W.-G. Bae, J. B.-H. Tok, Z. Bao, A chameleon-inspired stretchable electronic skin with interactive colour changing controlled by tactile sensing. *Nat. Commun.* **6**, 8011 (2015).
10. H. Kim, J. Choi, K. K. Kim, P. Won, S. Hong, S. H. Ko, Biomimetic chameleon soft robot with artificial crypsis and disruptive coloration skin. *Nat. Commun.* **12**, 4658 (2021).
11. P. Zhang, I. M. Lei, G. Chen, J. Lin, X. Chen, J. Zhang, C. Cai, X. Liang, J. Liu, Integrated 3D printing of flexible electroluminescent devices and soft robots. *Nat. Commun.* **13**, 4775 (2022).
12. W. R. Algar, C. A. De Jong, E. J. Maxwell, C. G. Atkins, Demonstration of the spectrophotometric complementary color wheel using LEDs and indicator dyes. *J. Chem. Educ.* **93**, 162–165 (2016).
13. S. Helmy, F. A. Leibfarth, S. Oh, J. E. Poelma, C. J. Hawker, J. Read de Alaniz, Photoswitching using visible light: A new class of organic photochromic molecules. *J. Am. Chem. Soc.* **136**, 8169–8172 (2014).
14. M. M. Lerch, W. Szymański, B. L. Feringa, The (photo) chemistry of Stenhouse photoswitches: Guiding principles and system design. *Chem. Soc. Rev.* **47**, 1910–1937 (2018).
15. J. R. Hemmer, S. O. Poelma, N. Treat, Z. A. Page, N. D. Dolinski, Y. J. Diaz, W. Tomlinson, K. D. Clark, J. P. Hooper, C. Hawker, J. Read de Alaniz, Tunable visible and near infrared photoswitches. *J. Am. Chem. Soc.* **138**, 13960–13966 (2016).
16. N. Mallo, P. T. Brown, H. Iranmanesh, T. S. C. MacDonald, M. J. Teusner, J. B. Harper, G. E. Balla, J. E. Beves, Photochromic switching behaviour of donor-acceptor Stenhouse adducts in organic solvents. *Chem. Commun. (Camb.)* **52**, 13576–13579 (2016).
17. Y. Duan, H. Zhao, G. Xue, F. Sun, F. Stricker, Z. Wang, L. Mao, C. He, J. Read de Alaniz, Y. Zheng, D. Wang, Controlling the isomerization of photoresponsive molecules through a limiting tautomerization strategy. *J. Phys. Chem. B* **126**, 3347–3354 (2022).
18. J. R. Hemmer, Z. A. Page, K. D. Clark, F. Stricker, N. D. Dolinski, C. J. Hawker, J. Read de Alaniz, Controlling dark equilibria and enhancing donor-acceptor Stenhouse adduct photoswitching properties through carbon acid design. *J. Am. Chem. Soc.* **140**, 10425–10429 (2018).
19. A. C. Overholts, W. Granados Razo, M. J. Robb, Mechanically gated formation of donor-acceptor Stenhouse adducts enabling mechanochemical multicolour soft lithography. *Nat. Chem.* **15**, 332–338 (2023).
20. F. Sun, X. Xiong, A. Gao, Y. Duan, L. Mao, L. Gu, Z. Wang, C. He, X. Deng, Y. Zheng, D. Wang, Fast photochromism in solid: Microenvironment in metal-organic frameworks promotes the isomerization of donor-acceptor Stenhouse adducts. *Chem. Eng. J.* **427**, 132037 (2022).
21. M. M. Sroda, F. Stricker, J. A. Peterson, A. Bernal, J. Read de Alaniz, Donor-acceptor Stenhouse adducts: Exploring the effects of ionic character. *Chem. Eur. J.* **27**, 4183–4190 (2021).
22. B. Schreiber, H. Martinek, P. Wolschann, P. Schuster, Kinetic studies on the nucleophilic addition to double bonds. 1. Addition of amines to electrophilic carbon-carbon double bonds. *J. Am. Chem. Soc.* **101**, 4708–4713 (1979).
23. F. Stricker, D. M. Sanchez, U. Raucci, N. D. Dolinski, M. S. Zayas, J. Meisner, C. J. Hawker, T. J. Martínez, J. Read de Alaniz, A multi-stage single photochrome system for controlled photoswitching responses. *Nat. Chem.* **14**, 942–948 (2022).
24. N. Mallo, E. D. Foley, H. Iranmanesh, A. D. W. Kennedy, E. T. Luis, J. Ho, J. B. Harper, J. E. Beves, Structure-function relationships of donor-acceptor Stenhouse adduct photochromic switches. *Chem. Sci.* **9**, 8242–8252 (2018).
25. O. Rifaie-Graham, J. Yeow, A. Najer, R. Wang, R. Sun, K. Zhou, T. N. Dell, C. Adrianus, C. Thanapongpibul, M. Chami, S. Mann, J. Read de Alaniz, M. M. Stevens, Photoswitchable gating of non-equilibrium enzymatic feedback in chemically communicating polymersome nanoreactors. *Nat. Chem.* **15**, 110–118 (2023).
26. F. Stricker, J. Peterson, S. K. Sandlass, A. de Tagyos, M. Sroda, S. Seshadri, M. J. Gordon, J. Read de Alaniz, Selective control of donor-acceptor Stenhouse adduct populations with non-selective stimuli. *Chem* **9**, 1994–2005 (2023).
27. D. F. Swinehart, The beer-lambert law. *J. Chem. Educ.* **39**, 333 (1962).
28. G. H. Jeffery, *Vogel's Textbook of Quantitative Chemical* (Wiley, 1989).
29. J. Schanda, *Colorimetry: Understanding the CIE System* (Wiley, 2007).
30. N. Ohta, A. Robertson, *Colorimetry: Fundamentals and Applications* (Wiley, 2005).
31. J. Alves, S. Wiedbrauk, C. Barner-Kowollik, J. P. Blinco, The missing piece: Concentration dependence of donor-acceptor Stenhouse adduct (DASA) reactivity. *ChemPhotoChem* **5**, 711–715 (2021).
32. B. F. Lui, N. T. Tierce, F. Tong, M. M. Sroda, H. Lu, J. Read de Alaniz, C. J. Bardeen, Unusual concentration dependence of the photoisomerization reaction in donor-acceptor Stenhouse adducts. *Photochem. Photobiol. Sci.* **18**, 1587–1595 (2019).
33. S. W. Connolly, R. Tiwari, S. J. Holder, H. J. Shepherd, A simple strategy to overcome concentration dependence of photoswitching properties in donor-acceptor Stenhouse adducts. *Phys. Chem. Chem. Phys.* **23**, 2775–2779 (2021).
34. R. S. Berns, *Billmeyer and Saltzman's Principles of Color Technology* (Wiley, 2019).
35. A. R. Robertson, Historical development of CIE recommended color difference equations. *Color Res. Appl.* **15**, 167–170 (1990).
36. G. Sharma, R. Bala, *Digital Color Imaging Handbook* (CRC Press, 2017).
37. F. Sun, D. Wang, Toward real-world applications: Promoting fast and efficient photoswitching in the solid state. *J. Mater. Chem. C* **10**, 13700–13716 (2022).
38. M. Clerc, S. Sandlass, O. Rifaie-Graham, J. A. Peterson, N. Bruns, J. Read de Alaniz, L. F. Boesel, Visible light-responsive materials: The (photo)chemistry and applications of donor-acceptor Stenhouse adducts in polymer science. *Chem. Soc. Rev.* **52**, 8245–8294 (2023).
39. X. Xiong, F. Sun, A. Gao, Z. Wang, Y. Duan, Z. Yao, C. He, R. Han, X. Deng, Y. Zheng, D. Wang, Ester matters? Promoting photoisomerization of donor-acceptor Stenhouse adducts in the solid state and "burn after reading" encryption. *Chem. Eng. J.* **450**, 138090 (2022).

Acknowledgments: We thank Y. Liu, C. S. Zhao, L. Q. Chen, H. Zhao, C. M. Xie, Q. Wei, B. He, X. D. Liu, and L. J. Mao for discussions. **Funding:** This work was supported by the National Natural Science Foundation of China (52203134, 62375041, and 22375029) and the Foundation of Science & Technology Department of Sichuan Province (2023ZYD0037, 2024YFHZ0307, and 2024NSFSC0249). **Author contributions:** Conceptualization: F.S. and D.W. Methodology: F.S. and D.W. Investigation: F.S., A.G., B.Y., H.Z., and D.D. Visualization: F.S., A.G., and B.Y. Image processing: B.Y. and J.Z. Funding acquisition: Y.Z., C.W., and D.W. Project administration: Y.Z., C.W., and D.W. Supervision: J.Z., X.W., X.D., Y.Z., C.W., and D.W. Writing—original draft: F.S. and D.W. Writing—review and editing: F.S., Y.Z., C.W., and D.W. **Competing interests:** The authors declare that they have no competing interests. **Data and materials availability:** All data needed to evaluate the conclusions in the paper are present in the paper and/or the Supplementary Materials.

Submitted 3 August 2024
Accepted 2 October 2024
Published 6 November 2024
10.1126/sciadv.ads2217